HHS Public Access

Author manuscript

Anal Methods. Author manuscript; available in PMC 2022 November 04.

Published in final edited form as:

Anal Methods. ; 13(42): 5017–5024. doi:10.1039/d1ay01569a.

Fully 3D printed Fluidic Devices with Integrated Valves and Pumps for Flow Injection Analysis

Andre D. Castiaux[a,b], **Major A. Selemani**[a], **Morgan A. Ward**[a], **R. Scott Martin**[a,b]

[a]Department of Chemistry, Saint Louis University

[b]Center for Additive Manufacturing, Saint Louis University

Abstract

The use of a PolyJet 3D printer to create a microfluidic device that has integrated valves and pumps is described. The process uses liquid support and stacked printing to result in fully printed devices that are ready to use within minutes of fabrication after minimal post-processing. A unique feature of PolyJet printing is the ability to incorporate several different materials of varying properties into one print. In this work, two commercially available materials were used: a rigid-transparent plastic material (VeroClear) was used to define the channel regions and the bulk of the device, while the pumps/valves were printed in a flexible, rubber-like material (Agilus30). The entire process, from initial design to testing takes less than 4 hours to complete. The performance of the valves and pumps were characterized by fluorescence microscopy. A flow injection analysis device that enabled the discrete injections of analyte plugs was created, with on-chip pumps being used to move the fluid streams. The injection process was found to be reproducible and linearly correlated with changes in analyte concentration. The utility was demonstrated with the injection and rapid lysis of fluorescently-labeled endothelial cells. The ability to produce a device with integrated pumps/valves in one process significantly adds to the applicability of 3D printing to create microfluidic devices for analytical measurements.

Graphical Abstract

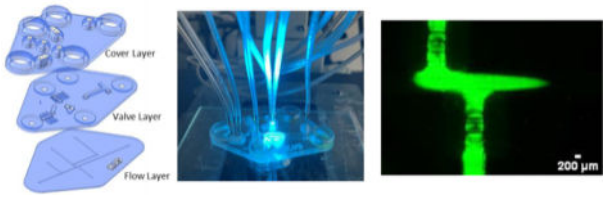

The use of a PolyJet 3D printer to create a microfluidic device that has integrated valves and pumps is described. A flow injection analysis device that enabled the discrete injections of analyte plugs was created, with on-chip pumps being used to move the fluid streams.

*corresponding author: Prof. R. Scott Martin, Department of Chemistry and Center for Additive Manufacturing, 3501 Laclede Ave., St. Louis, MO, USA 63103, +1 314-977-2836, scott.martin@slu.edu.

Supplemental Information

Supplemental information contains all the STL files used for the 3D printing, videos of the pumps in action and an injection sequence, and Figs. S1 and S2.

Introduction

The ability to 3D print microfluidic devices has the potential to drastically improve and streamline the fabrication process and aid in bringing more devices to the mainstream. Since the late 1970s when Terry *et al.* first realized a miniaturized gas chromatography system,[1] the idea of a fully integrated lab-on-a-chip device has been seen as the ideal end-stage for analytical meaurements.[2,3] Ideally, such devices would integrate multiple processes to enable sample-in/answer-out capabilities on complex real-world samples.[4] However, a majority of these devices rely on a complex, costly, and specialized fabrication process that has helped to limit widespread adoption of the technology.[5] Clearly, new approaches are needed to rapidly mass produce robust devices of sufficient complexity.

Microfluidic device fabrication has evolved rapidly over the last 40 years. Initial approaches involved the use of lithography and wet etching steps to fabricate devices in glass or silicon.[6] Soft lithography approaches are popular and involve using photolithography to pattern the desired design on a silicon wafer (i.e. master), followed by covering this master in an elastomer such as PDMS. The elastomer can then be delaminated leaving the desired pattern.[7] The processes used to make these devices can be complex, and changing a design can often take days due to requirement of a new mask and master. Alternative methods have been developed using machining or embossing of plastics, which involves significant investment in both equipment and expertise.[8,9] In terms of fluid handling, the Quake group first reported all PDMS devices with valves and pumps.[10,11] Separate control and flow layers were fabricated and then sealed together to result in highly integrated devices that could do 400 independent reactions.[12] These “Quake-style valves” have been utilized in glass devices (using a thin PDMS membrane)[13,14] and hybrid PDMS/glass devices.[15]

One rising technology with the potential to simplify and universalize microfluidic device fabrication is additive manufacturing (commonly referred to as 3D printing).[16–18] While several techniques fall under the umbrella of additive manufacturing, each technique utilizes a base material to build up a model in a layer-by-layer fashion. The base materials for fused deposition modeling (FDM) are thermoplastics, for vat polymerization and PolyJet printing it is photocurable resins, and for selective laser sintering (SLS) it is a bed of powder. With 3D printing, ideas can be quickly designed in CAD software and programed into any one of the additive techniques described above, with production times from design to product in hand being possible in a few hours per iteration. Once a final design is found, it can easily be shared to any researcher or manufacturer with a system of comparable resolution. Given the large number of printers available in private and educational settings, devices can be more readily available and even selective manufacturing in remote areas can be done by employing small additive systems.

Vat polymerization, FDM, and PolyJet printing have all emerged as viable additive manufacturing technologies for microfluidics over the past 5 years. Vat polymerization, using techniques such as stereolithography or “SLA”, has been used because of its high-resolution and limited post-processing requirements. A basic vat polymerization system can easily print complex enclosed channels in the sub mm range, with high-end and custom systems achieving resolution down to 10’s of microns;[19,20] however, these systems result in

devices made of a single material type. In terms of creating integrated devices with valves and pumps for fluid handling, the Woolley and Nordin groups were able to use a custom high-resolution SLA printer to selectively cure the resin and achieve variable material properties throughout the system.[21,22] This enabled the fabrication of devices with high density pumping/valving components, albeit with a small build size and limited material options. Other researchers have SLA printing with a specially formulated poly(ethylene glycol) diacrylate-based resin to produce on-chip valves and pumps.[23] Another viable technique is FDM 3D printing. This technique carries the lowest cost to entry, often in the range of thousands of USD's or less.[24–26] However, since this technique relies on bonding liquified thermoplastics, significant challenges exist with manufacturing optically clear and liquid tight devices. Finally, material jetting, also known by the trade name PolyJet printing, is another viable technology for the fabrication of microfluidic devices. PolyJet printing has the distinct advantage of being able to easily incorporate multiple materials into a single model. This enables the fabrication of rigid microfluidic devices that can be transparent and also include selective regions or layers that contain rubber like materials. Until recently, in order to make full enclosed microfluidic channels with material jetting one had to mechanically remove solid support material. This limits the channel size and network complexity.[27] One work around to the limitations presented by support removal for valving devices is to fabricate the components of the valve in separate pieces and then assemble the final device in post processing, as shown by Keating et al.[28] However, this limits the ability to quickly mass produce microfluidic devices of this style in one print process.

In this paper, a PolyJet 3D printer was used to create a microfluidic device that has integrated valves and pumps. The process builds upon our recently described approach of liquid support and stacked printing[27] to result in fully printed devices that are ready to use with minimal post-processing. A unique feature of PolyJet printing is the ability to incorporate several different materials of varying properties (transparency, color, durometer) into a single device. Here, the majority of the device is printed with a hard and transparent plastic material (VeroClear), with channel regions where a valving action is desired being covered with a flexible, rubber-like material (Agilus30). The entire process, from initial design to testing, takes less than 4 hours to complete (Fig. 1). The performance of the valves and pumps were characterized by fluorescence microscopy. A flow injection device that enabled the discrete injections of analyte plugs was created, with on-chip pumps being used to move the fluid streams. The injection process was found to be reproducible, and the utility was demonstrated with the injection and rapid lysis of fluorescently labeled endothelial cells.

Experimental

Materials and methods

Isopropyl alcohol was obtained from Thermo-Fisher Scientific (St Louis, MO). Glycerol, sodium dodecyl sulfate (SDS), acridine orange and Tween20 were purchased from Sigma Aldrich (St. Louis, MO). VeroClear and Agilus30 were purchased from Stratasys (Eden Prairie, MN). Liquid support for the 3D printer was either pure Tween20 or a 60:40 (by volume) mixture of Glyrcol:IPA.

Device Design and Fabrication

All devices were designed in Autodesk Inventor Professional 2021 (Autodesk, Inc., San Rafael, CA) or comparable CAD software. Chips were designed in single part files with different bodies representing each layer and different materials. These bodies were then exported as an assembly to six STL files. These six files are broken down into two STL files per layer (with the 3 layers being a Flow Layer, Valve Layer, and Cover Layer), with one STL for the Agilus30 component and one for the VeroClear material. The top-down view of the device is in Fig. 2A, with the exploded view of the layers being seen in Fig. 2B (blue color representing material printed in Veroclear and white presenting the material printed in Agilus30). While the chip was designed in CAD as separate layers, it was fabricated as a completed chip using a stacked print approach on a Stratasys J735 Polyjet 3D printer.[27] When the print process was complete, the chips were removed from the print bed, channels cleaned with compressed air followed by water, and then the bottom of the chip was painted with nail polish (Sally Hansen No Chip Acrylic) to increase transparency of the device.

Fig. 2B outlines the 3 different layers used to print the device. The flow layer contained the base of the chip and the flow channels that the pumps and valves control. This section had a height of 0.840 mm, of which 0.540 mm was the base and 0.300 mm was the height of the channels. All channels in this layer were designed to be 600 μm in width × 300 μm tall, with a circular base. Fig. S1 contains a micrograph of the resulting printed channel cross-section, with the final channels being smaller than designed, as seen previously with the use of the liquid support[27] and in other studies using PolyJet printing to fabricate enclosed channels.[29] The valving layer was printed directly on top of the flow layer after adding Tween20 into the open channels (as a liquid support). The valving layer was designed to be 1.28 mm in height, with a printed Agilus30 membrane that is 0.280 mm in thickness. A valving/pneumatic channel (that is pressurized when valving action is desired) resides on top of the valving layer, with CAD dimensions of either 1.2 mm or 1.8 mm in width (depending on which valve the channel controlled.) × 1.0 mm in height. All channels in this layer were designed to have a square cross-sectional profile. During the printing process, the pneumatic channels are filled with liquid support (60:40 Glycerol: IPA, v/v) before printing the cover layer. Finally, the cover layer was designed to conserve material by making the bulk of the layer 1 mm in thickness except for the 2 mm directly surrounding the Agilus 30 connection ports and the reservoirs, both of which were printed to be 5 mm in thickness. The reservoirs were designed to be 10 mm in diameter and could hold up to 400 μL of liquid. The Agilus30 connection ports to interface with the gas tubing were designed at the same dimensions as previously reported (0.750 mm ID × 2.5 mm OD and 5 mm height[27]).

Two valve sizes were used in this device. It should be noted that these are push-down valves, where pressure is used to push the Agilus valving layer down into the underlying flow channel. A smaller valve was used for the embedded peristaltic pumps, with CAD dimensions of 600 × 1200 μm over the flow channel (full dimensions shown in Fig. 3A). The pumps were comprised of three individually addressable valves, designed to be spaced at 600 μm along the fluidic channel. A larger valve was designed (Fig. 3E) in order to be fully closeable and direct fluid flow through the system (i.e. injection valves). This larger Agilus valve was designed in CAD to be 1800 × 600 μm. All the valves were designed

at 0.280 mm thick (of Agilus). This Agilus material was then actuated with nitrogen and pushed down into the flow channels. When the pressure was released, the Agilus valving layer released out of the channel.

Device Operation

Connections to the pneumatic channels was accomplished with Agilus30 gaskets similar to what was previously reported for fluid connections.[27] In short, a ½" 20 Ga needle was purchased from Amazon and the steel pin removed. One side of the pin was inserted into the Agilus30 connection port (Fig. 3A) and the other side was connected to tubing from valve controller. The peristaltic pumps were operated at 30 psi using an eight-channel valve controller from Fluidigm (San Francisco, CA). As previously reported, this controller allows for pump operation at programmable peristaltic pump sequence frequencies.[30] The same controller was used to apply pressure to the injection valves, where one set is normally closed and the other set normally open. When actuated, these states reverse. To visualize the pump/injection sequence, the device was placed on to an inverted fluorescence microscope (Olympus IX71) fitted with a 2X objective (Olympus PLN2X, Japan). Images and videos were taken with a Lumenera INFINITY2 (Teledyne Lumenera, Ontario, Canada) digital CCD camera. All reservoirs were filled with the same volume of solution (200 μL) for these studies.

Fig. 4 outlines experiments to demonstrate the closing of the pumps (Fig. 4A and C) and injection (Fig. 4B and D) valves. In this experiment, the channels were filled with a 1 mM fluorescein solution and the valve pressure was gradually increased with 5 psi increments for each measurement up to 30 psi (fresh solution was introduced into the channel between each pressure change). The fluorescence intensity under each valve was measured with the windows shown in the figure using ImageJ.

Fig 5A shows the annotated CAD rendering of the device used for microchip-based flow injection analysis, with integrated pumps and valves being used to load and inject sample. In terms of device operation, the sample channel was filled with the desired solution, and the analysis channel with deionized water. Vacuum was used to remove bubbles from the channels. The peristaltic pump sequence was set at frequency 2 Hz for both the sample and analysis pumps. During the loading step, the analysis pump was switched off, normally open injection valves were closed and the normally closed injection valves opened, allowing sample to flow from the sample reservoir to injection waste (filling up the junction loop, see Fig. 5B). During the injection step, the valve states are reversed, and the analysis pump is activated to pump the resulting injection plug down the analysis channel, towards the analysis waste reservoir (Fig. 5B). A video of the injection moving through the system is included in the supporting documentation.

To assess the robustness of the injection process, a calibration curve was generated using known concentrations of five solutions of fluorescein (100, 250, 500, 750, and 1000 μM). These were all prepared from a standard stock fluorescein solution (10 mM) and diluted with a 50 mM sodium phosphate buffer (pH = 7.2). Injections and analysis were performed in triplicate for each concentration. The plug migration in the analysis channel was recorded as a video sequence (in avi format) and a video processing code in MatLab

and Simulink software (R2021a) was used to analyze and determine the mean fluorescence intensity in a region of interest (ROI) over time. The detection window dimensions (0.9 mm × 1.6 mm), and the position (15 mm from junction) was kept the same for all the calibration measurements. The average peak height for each concentration was plotted against concentration (Fig. 5C).

For the cell lysis experiments (Fig. 6), bovine pulmonary arterial endothelial cells (BPAECs) from ATCC were cultured in T-75 culture flasks until they were 80% confluent, as previously described.[31,32] The BPAECs were then stained with a 0.1 mM acridine orange solution (pH = 7.4) and were resuspended after sub-culturing to a final concentration of ~1×10^6 cells/mL, following previously described protocols.[33,34] The sample reservoir was filled with 200 μL of the stained BPAEC solution and the analysis channel was filled with a 50 mM solution of sodium dodecyl sulfate (SDS). The BPAECs were then pumped to the sample waste reservoir. The naturally closed valves were opened to load the stained BPAECs into the analysis channel (Fig. 6A). After injection, the plug of stained cells were pumped down the analysis channel, where they are lysed by the SDS solution.

Results and Discussions

Device Fabrication

A limitation of Polyjet printers is the requirement of support material to print enclosed structures. Polyjet 3D printers utilize inkjet print heads and jet liquid photocurable resin. Each layer of droplets must have a supporting layer underneath, otherwise the droplets will deposit into the underlying layer before the UV curing step (filling any channel network). With the Stratasys PolyJet systems, the printer is only capable of using a waxy-like sacrificial support material that is semi-soluble in a caustic bath and requires some mechanical removal of support. This limits the channels sizes and the complexity of the fluidic design. As reported previously, one way around this limitation is to utilize non-printed liquid support materials.[27] By stacking the layers during the printing process, the channels are left exposed so that they can be filled with a liquid support material that can easily be removed by vacuum or pressure when printing is complete. In this work, a solution of Tween 20 was used for the liquid support when making smaller fluidic channels (designed to be 600 × 300 μm) in the flow layer, with a 60:40 Glycerol:IPA solution being used as the liquid support for the larger pneumatic channels in the valving layer. Fig. S1 shows a micrograph of the resulting printed fluidic channel cross-section, with the printed channels being smaller than designed in CAD, as seen previously.[27,29] Fig. 2A shows the top-down view of the fully assembled chip with channels colorized for clarity. The fluid flow path and connected reservoirs are shown in green while the pneumatic channels for actuating the valves are shown in red. These green and red regions are filled with the appropriate liquid support material in between printing each layer. This liquid is then easily flushed from the flow layer with vacuum or compressed air (Fig. 1). The liquid supports are left in the pneumatic channel and do not affect the function of the valves. Fig. 2C shows a fully printed device that is ready for use

Characterization of Valves/Pumps

The valves used in this study are of the push down variety, where the overlying valve layer, when pressurized, compresses down into the flow channel. As opposed to PDMS valves, which are normally dead-end filled with a liquid due to the gas permeable nature of PDMS, the 3D printed valves used here could be actuated directly with a gas (since the materials are not gas permeable[35]). Two valve sizes were used in this device, one for the valve used as pumps (Fig. 3A) and another for the valves used to control fluid direction (injection valves, Fig. 3E). In terms of the Agilus/valving layer, to ensure rapid valve actuation (important especially for the pumps), the goal was to have as thin of a layer as possible. The thickness of this layer was designed to be 0.280 mm. Thinner layers (0.200 mm) were investigated but a high rate of valve failure/rupture was seen. Larger (thicker) layers were not investigated.

A smaller valve was used for the embedded peristaltic pumps, with CAD dimensions of 600 × 1200 μm over the flow channel. The pumps were comprised of three individually addressable valves designed to be spaced at 600 μm along the fluidic channel. Closer spacings were not possible (the channels were not fully separated after printing) and large spacings led to reproducibility issues with pumping. Fig. 3B shows a fluorescein filled channel with all three pumping valves open. In contrast Fig. 3C shows all three pumping valves in the closed position. Finally, Fig. 3D shows valve 1 and 3 closed and valve 2 open. A video of the pumps in action at 2 Hz is included in the supplemental information. A set of larger valves (600 × 1800 μm) were designed in CAD to be fully closeable and direct fluid flow through the system. These valves (dimensions shown in Fig. 3E) enabled injections of analyte into the device and operated to either be normally closed or normally open (depending on how flow direction is routed). Since these valves are always opened or closed in tandem, each set was operated from one pneumatic line (see Fig. 5A). This aided by the rigid nature of the 3D printed plastic material. Fig. 3F shows these two valves open while Fig. 3G shows both closed (channels filled with fluorescein for visualization purposes).

To characterize the closure of the two valve types used here (pumps and injection valves), the flow channels were filled with a 1 mM fluorescein solution and increasing pressure was applied from the pneumatic control system to each valve at the same time. New fluorescein solution was added to the region under investigation between each measurement. The intensity of the fluorescent signal in the ROI detection window (0.8 mm × 1.5 mm) was analyzed, with all signals normalized to the intensity of the valves with no pressure applied (0 psi). Fig. 4A and 4B show the regions that were measured for the pumping valves and injection valves, respectively (see colored boxes). Fig. 4C shows the results for up to 30 psi being applied to the pumping valves. As pressure is increased the intensity decreases due to less fluorescein being present under the pump valves. While the signal does not plateau at the higher pressures these valves were not designed to fully close, which is common for peristaltic pump-type valves due to the need to continuously cycle their operation (for pumping action). Sufficient pumping action was achieved at 30 psi, so this pressure was used for further work. Fig. 4D shows the results for the same conditions being applied to the larger injections valves. Since these valves are significantly larger, a plateau was reached after 20 psi suggesting adequate closing of these valves (the injection plug work in the next

section also supports this). It was also found that once 55 psi of pressure was applied to the injection valves, the device began to delaminate between the valving and flow layers ($n=3$). Since all connections were robust enough for 30 psi of applied pressure, this pressure was used for all studies going forward.

Flow Injection Analysis

The flow injection analysis process used here had 2 separate steps, a loading step (where sample is directed into the analysis channel in a defined plug region), and an injection step (where the plug is carried down the analysis channel to a detection window). Prior to the loading step, the sample is pumped (2 Hz pump frequency) from the sample reservoir to the sample waste reservoir while deionized water is pumped at the same frequency from the analysis reservoir to the analysis waste. The injection valves that help to define the injection plug are normally closed (blue label in Fig. 5A). During the loading step, these valves are opened for 15 sec (normally open valves being pressurized to close, red outline in Fig. 5B), with the analysis pump valves being turned off; this forces liquid to fill the sample loop (Fig. 5B). After this period of time, these states are reversed, the analysis pumps turned back on, and the injected plug is directed down the analysis channel, towards the detection window.

To test the functionality of the design, varying concentrations of fluorescein (100–1000 μM) were loaded in the sample reservoir and injected into the analysis channel. A 0.9 mm × 1.6 mm detection window was placed 15 mm from injection region and the fluorescence measured as a function of time through a 2X objective. The resulting calibration curve is shown in Fig. 5C. A good correlation is seen, with the inset showing an overlay of 3 separate injections of a 250 μM fluorescein solution (% RSD = 2.9%). The injection plug volume was measured to be 300 nL when taking into account the channel cross sectional area (Fig. S1A) and the length of the injection plug (Fig. S1 B). The injection volume can be tuned by adjusting the spacing between the incoming sample channel and the outgoing injection channel. For determination of linear velocity, 7 consecutive injections of a 1 mM fluorescein were performed and the time it took for these plugs to transverse down the analysis channel to the detection window (15 mm) was recorded (time the peak started to elute). The calculated average linear velocity was 0.04 ± 0.002 cm/s. Considering the channel cross sectional area shown in Fig. S1A (8.2×10^{-4} cm^2), this equates to a volumetric flow rate of 2.0 μL/min in the analysis channel. Finally, the effect of the pump frequency was investigated, as shown in Fig. S2. Pump frequencies between 2–4 Hz led to well defined peaks that eluted in a reasonable time.

Manipulating cellular samples is a common application of microfluidic devices. Fig. 6 shows the ability to use this flow injection analysis design to perform injection of a cell sample and on-chip lysis. Buffers for cell lysis differ in their ability to solubilize proteins, with those containing sodium dodecyl sulfate (SDS) and other ionic detergents considered to be the most efficient in achieving protein solubility.[36] In this experiment, the analysis channel was filled with a 50 mM solution of SDS and the sample reservoir was filled with fluorescently-labeled endothelial cells. A schematic of the device is shown Fig. 6, with optical images of fluorescently-labeled endothelial cells at various stages of the lysis process also shown in the figure. A plug of labeled cells was injected into the analysis channel and

begin to lyse as they are pumped down the channel (as they encounter the SDS solution). As shown in the figure, the lysis process was complete within ~22 sec of plug injection.

Conclusions

A limitation of traditional microfluidic device fabrication is the ability to rapidly iterate designs and then mass produce a final product. The PolyJet-based 3D printing approach described herein for integrating valves and pumps has the ability to rapidly iterate designs in a fashion where the final device is ready for use with minimal post-processing. The valves and pumps were characterized with fluorescence microscopy and their applicability was shown by creating a microchip-based flow injection analysis device. Discrete injections of liquid and cellular samples were possible. In this paper, we reported the ability to iterate through at least one design per day. If desired, the final design could be easily transferred to a similar 3D printer or a service bureau with the appropriate technology. In terms of scaling, with just one J735 printer, 64 chips could be made in one day for less than $6 USD per chip. While limitations of this approach does exist (including resolution and the manual addition of liquid support), advancements in 3D printing are rapidly occurring. The print heads used in these systems are still relatively low resolution at about 600 dpi in the x axis and 300 dpi in the y axis. Higher resolution print heads do exist[37] and as they are further incorporated into commercially available 3D printing technology, smaller channel sizes could be realized. Finally, as the technology continues to mature, the cost will continue to drop (it should be noted that the cost estimate given here was for a top of the line system). This work, along with previous work from our labs on using stacked printing and liquid supports to encapsulate capillary tubing as well as electrodes for sensing,[38] clearly shows that PolyJet technology affords a versatile approach to mass produce highly functional and integrated analytical devices.

Supplementary Material

Refer to Web version on PubMed Central for supplementary material.

Acknowledgments

The authors would like to thank Emily Currens for help with the cell experiments. The authors would like to acknowledge Saint Louis University’s Center for Additive Manufacturing (SLU-CAM) for providing access to the Stratasys J735 Polyjet 3D printer. The work was funded by the National Institutes of Health (2R15GM084470 05A1).

References

1. Terry SC, Jerman JH and Angell JB, IEEE Transactions on Electron Devices, 1979, 26, 1880–1886.
2. Abgrall P and Gué AM, J Micromech Microeng, 2007, 17, R15–R49.
3. Whitesides GM, Nature, 2006, 442, 368–373. [PubMed: 16871203]
4. Le Roux D, Root BE, Hickey JA, Scott ON, Tsuei A, Li J, Saul DJ, Chassagne L, Landers JP and de Mazancourt P, Lab Chip, 2014, 14, 4415–4425. [PubMed: 25248520]
5. Rios A, Zougagh M and Avila M, Anal Chim Acta, 2012, 740, 1–11. [PubMed: 22840644]
6. Harrison DJ, Manz A, Fan Z, Luedi H and Widmer HM, Anal Chem, 1992, 64, 1926–1932.
7. Duffy DC, McDonald JC, Schueller OJA and Whitesides GM, Anal Chem, 1998, 70, 4974–4984. [PubMed: 21644679]

8. Soper SA, Ford SM, Qi S, McCarley RL, Kelly K and Murphy MC, Anal Chem, 2000, 72, 642A–651A.
9. Weerakoon-Ratnayake KM, O'Neil CE, Uba FI and Soper SA, Lab Chip, 2017, 17, 362–381. [PubMed: 28009883]
10. Fu AY, Chou H-P, Spence C, Arnold FH and Quake SR, Anal Chem, 2002, 74, 2451–2457. [PubMed: 12069222]
11. Unger MA, Chou H-P, Thorsen T, Scherer A and Quake SR, Science, 2000, 288, 113–116. [PubMed: 10753110]
12. Liu J, Hansen C and Quake SR, Anal Chem, 2003, 75, 4718–4723. [PubMed: 14674446]
13. Karlinsey JM, Monahan J, Marchiarullo DJ, Ferrance JP and Landers JP, Anal Chem, 2005, 77, 3637–3643. [PubMed: 15924399]
14. Kim J, Kang M, Jensen EC and Mathies RA, Anal Chem, 2012, 84, 2067–2071. [PubMed: 22257104]
15. Li MW, Huynh BH, Hulvey MK, Lunte SM and Martin RS, Anal Chem, 2006, 78, 1042–1051. [PubMed: 16478094]
16. Chen C, Mehl BT, Munshi AS, Townsend AD, Spence DM and Martin RS, Anal Methods, 2016, 8, 6005–6012. [PubMed: 27617038]
17. Au AK, Huynh W, Horowitz LF and Folch A, Angew Chem, 2016, 55, 3862–3881. [PubMed: 26854878]
18. Weisgrab G, Ovsianikov A and Costa PF, Adv. Mater. Technol, 2019, 4, 1900275.
19. Beauchamp MJ, Nielsen AV, Gong H, Nordin GP and Woolley AT, Anal Chem, 2019, 91, 7418–7425. [PubMed: 31056901]
20. Gong H, Bickham BP, Woolley AT and Nordin GP, Lab Chip, 2017, 17, 2899–2909. [PubMed: 28726927]
21. Gong H, Woolley AT and Nordin GP, Lab Chip, 2016, 16, 2450–2458. [PubMed: 27242064]
22. Rogers CI, Qaderi K, Woolley AT and Nordin GP, Biomicrofluidics, 2015, 9, 016501. [PubMed: 25610517]
23. Lee YS, Bhattacharjee N and Folch A, Lab Chip, 2018, 18, 1207–1214. [PubMed: 29553156]
24. Tothill AM, Partridge M, James SW and Tatam RP, J Micromech Microeng, 2017, 27.
25. Bressan LP, Adamo CB, Quero RF, de Jesus DP and da Silva JAF, Anal Methods, 2019, 11, 1014–1020.
26. Quero RF, Domingos da Silveira G, Fracassi da Silva JA and Jesus DP, Lab Chip, 2021.
27. Castiaux AD, Pinger CW, Hayter EA, Bunn ME, Martin RS and Spence DM, Anal Chem, 2019, 91, 6910–6917. [PubMed: 31035747]
28. Keating SJ, Gariboldi MI, Patrick WG, Sharma S, Kong DS and Oxman N, PLoS One, 2016, 11, e0160624. [PubMed: 27525809]
29. Macdonald NP, Cabot JM, Smejkal P, Guijt RM, Paull B and Breadmore MC, Anal Chem, 2017, 89, 3858–3866. [PubMed: 28281349]
30. Bowen AL and Martin RS, Electrophoresis, 2010, 31, 2534–2540. [PubMed: 20665914]
31. Selimovic A and Martin RS, Electrophoresis, 2013, 34, 2092–2100. [PubMed: 23670668]
32. Townsend AD, Sprague RS and Martin RS, Electroanalysis, 2019, 31, 1409–1415. [PubMed: 32999581]
33. Polunovsky VA, Wendt CH, Ingbar DH, Peterson MS and Bitterman PB, Exp Cell Res, 1994, 214, 584–594. [PubMed: 7925652]
34. Phillips PG and Tsan MF, J Histochem Cytochem, 1988, 36, 551–554. [PubMed: 3356897]
35. Levitsky Y, Pegouske DJ, Hammer SS, Frantz NL, Fisher KP, Muchnik AB, Saripalli AR, Kirschner P, Bazil JN, Busik JV and Proshlyakov DA, RSC Advances, 2019, 9, 33257–33267. [PubMed: 32123561]
36. Elinger D, Gabashvili A and Levin Y, J Proteome Res, 2019, 18, 1441–1445. [PubMed: 30761899]
37. Dixon C, Lamanna J and Wheeler AR, Adv. Mater. Technol, 2017, 27, 1604824.
38. Castiaux AD, Currens ER and Martin RS, Analyst, 2020, 145, 3274–3282. [PubMed: 32242194]

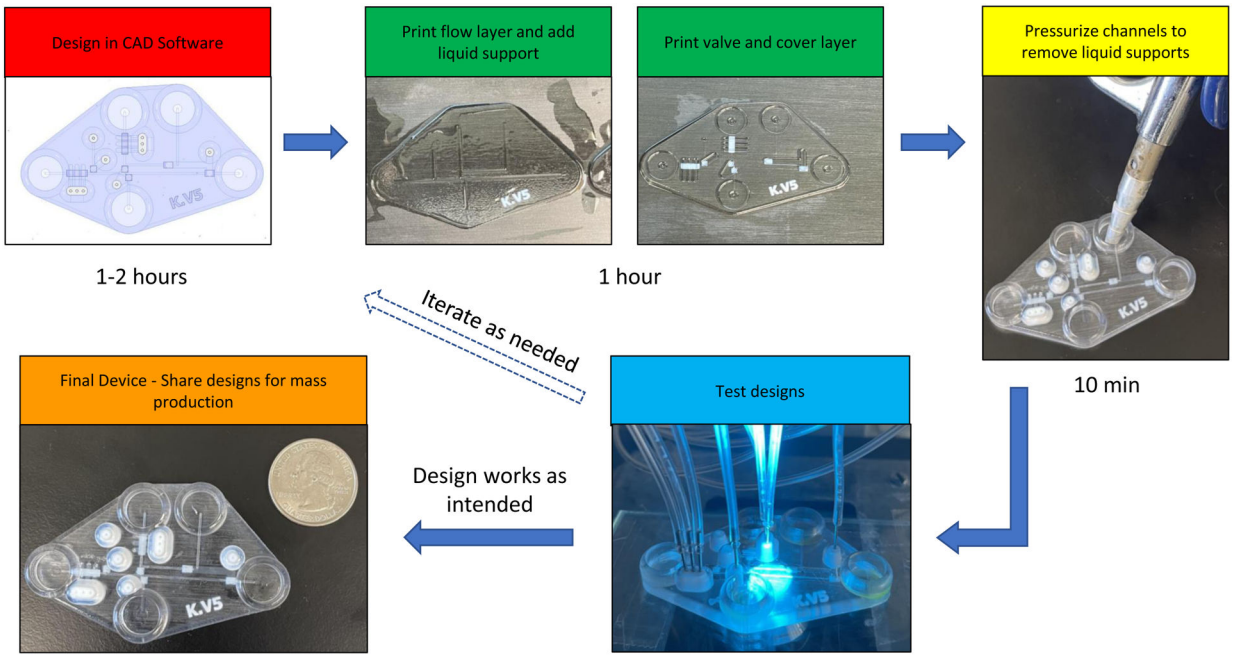

Figure 1.

Fabrication procedure used for the multi-layer, 3D printed devices used in these studies. Designs made in CAD are printed in several steps. A flow layer is printed first, liquid support is added, and separate prints for valving (containing white Agilus 30 where valving is needed) and cover layers are completed. Air is used to pressurize channels and remove liquid support. Designs are tested on a microscope and, if needed, designs can be changed in CAD and the process repeated in a relatively short time frame. The final device is down with respect to a US quarter.

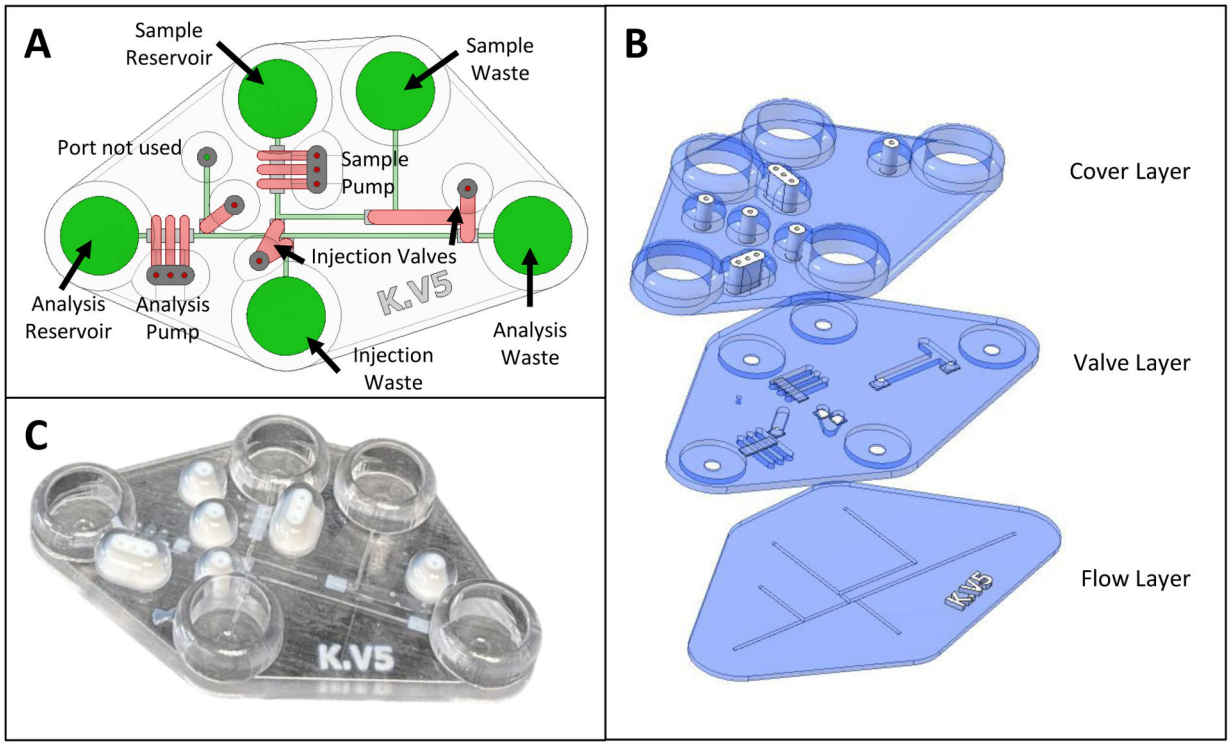

Figure 2.

CAD schematics and picture of final device. (A) Annotated CAD rendering (top-down view) of fully assembled chip, with pumps and valves in red and the flow layer in green. (B) Exploded CAD rendering showing the three layers required to fabricate the chip by support free Polyjet printing. White regions denote Agilus30 (rubber-like material) with other regions being made with VeroClear 3D printing resin. The flow (bottom) layer has the fluidic network. The valving (middle) layer contains a 280 μm thick Agilus valve (where desired) as well as the channel network to actuate those valves. The cover (top) layer has fluidic reservoirs that give access to the flow layer as well as pressure-based fittings to connect gas lines for the valves/pumps. (C) Picture of a fully fabricated chip showing the different materials that were used.

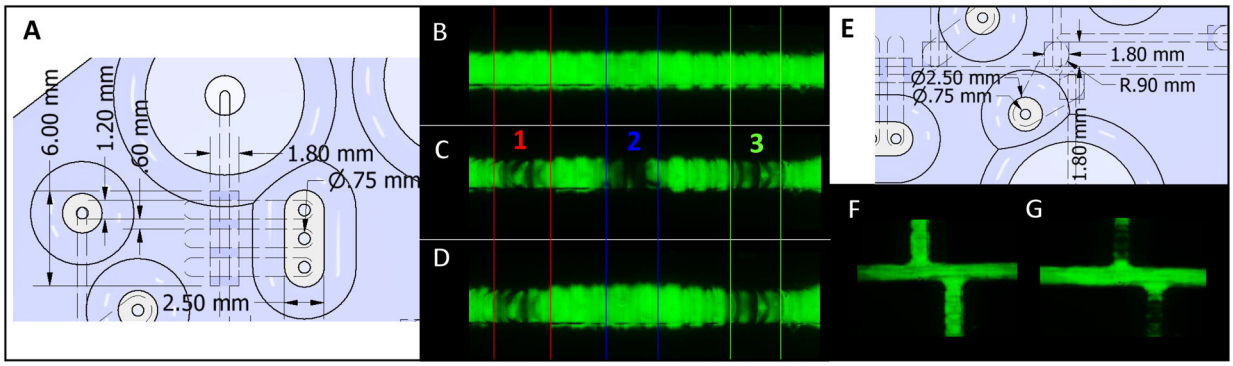

Figure 3.

CAD and fluorescent images showing the pumping and injection valves. (A) Annotated dimensions (mm) of the pumping valves with white representing the rubber like Agilus30 and blue representing hard plastic (Vero Clear). (B) Micrograph of fluorescein filling the channel under the pumping valves, with all three valves open. (C) Micrograph of fluorescein filling channel under the pumping valve with all three valves closed (30 psi of applied pressure). (D) Similar micrograph of valve 1 and 3 closed and valve 2 open. (E) Annotated CAD dimensions (mm) of the injection valves, with white representing the rubber like Agilus30 and blue representing the hard plastic (Vero Clear). (F) Micrographs showing injection valve open and, (G) the injection valve closed.

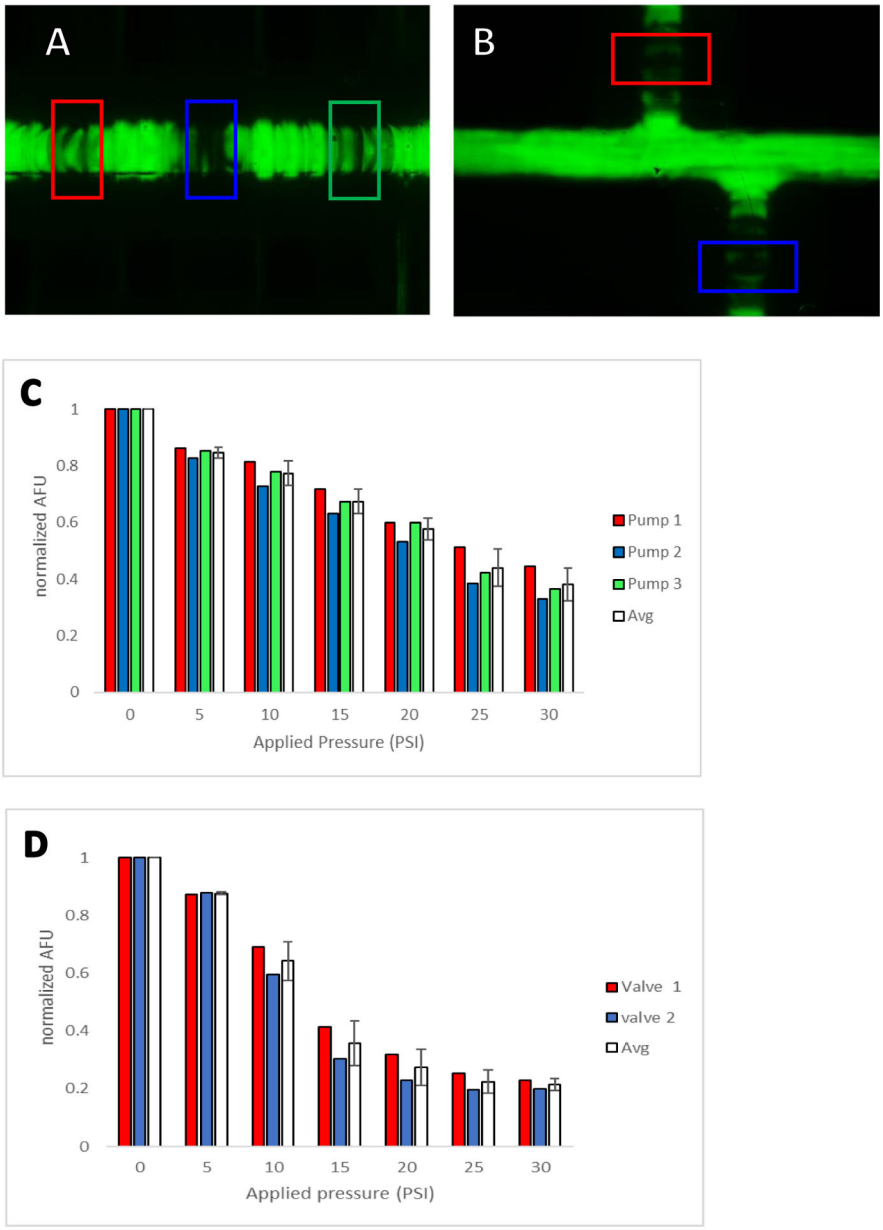

Figure 4.

Fluorescence characterization of closing the pumps/valves. (A) Pumping valves with regions of analysis (detection windows) denoted in red, blue, and green. (B) Injection valves with regions of analysis (detection window) denoted in red and blue. (C) Plot of relative fluorescence intensity for each pump valve vs. increased applied pressure. Average normalized fluorescence for the all 3 pumping valves are shown in white. (D) Plot of relative fluorescence intensity for both injection valves vs. increased applied pressure. Average normalized fluorescence for the valves shown in white.

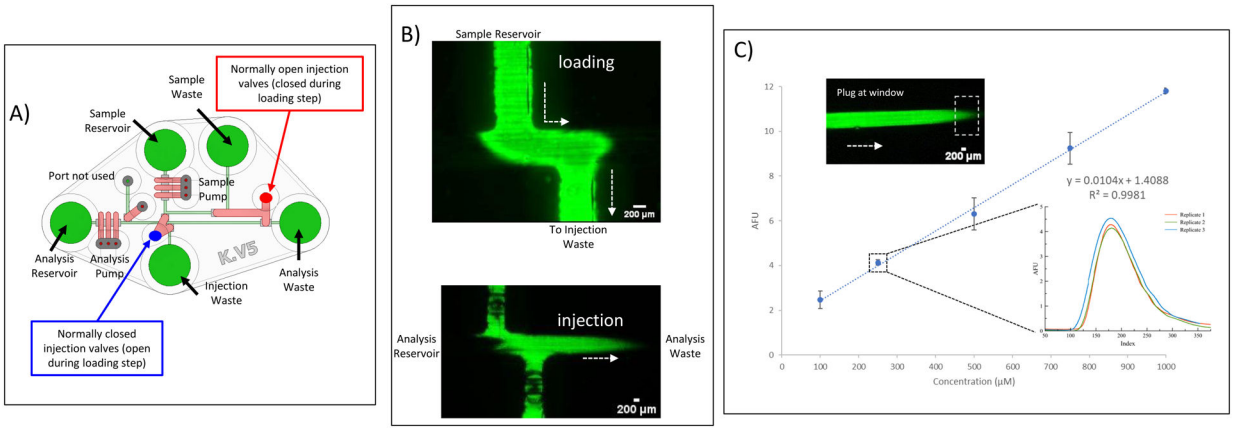

Figure 5.

Loading and Injection of Sample with the pumps and valves. A) Annotated CAD rendering (top-down view) of fully assembled chip, with specific labels of which valves are normally open (during injection/analysis step) and which are normally closed. During the loading/fill step, the valve states are reversed. B) Fluorescence micrographs of loading and injection process, with the loading micrograph being taken at the sample/analysis channel intersection and the injection micrography just downstream from the intersection. Injection volume is 300 nL. C) Calibration curve for injections of various fluorescein concentrations (100 – 1000 µM), with the plot inset containing an overlay of 3 separate injections of a 250 µM fluorescein solution. Micrograph shows plug at the detection window (outlined with dotted box).

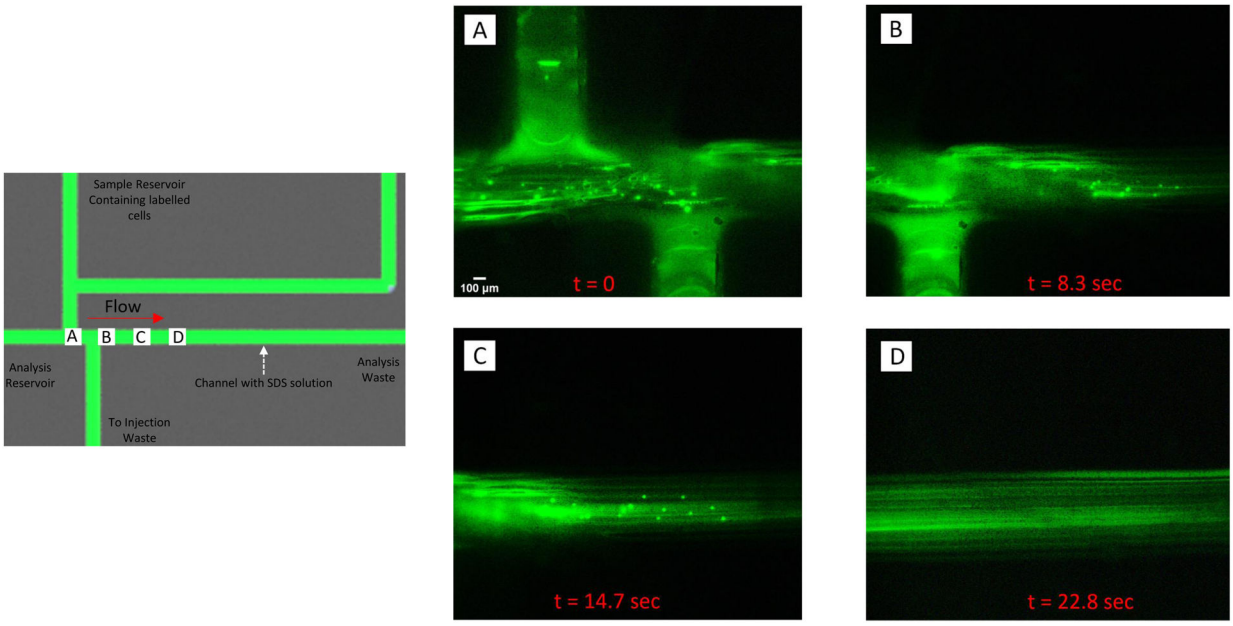

Figure 6.

Injection and lysis of a plug of fluorescently-labeled endothelial cells. The schematic contains labels (A-D) that correspond to the location where the fluorescent micrographs were taken. Bovine pulmonary endothelial cells were incubated with acridine orange (intracellular dye) and added to the sample reservoir. As shown in A), cells were pumped into the device and, when analysis was desired, directed towards the injection waste by actuating the injection valves. The analysis channel contained a 50 mM solution of sodium dodecyl sulfate (SDS) and when a plug of cells where injected into the channel, they started to lyse (B and C). Complete lysis occurred ˜22 sec after the injection process was initiated (D).